





Efficient strain modulation of 2D materials via polymer encapsulation

Zhiwei Li¹, Yawei Lv¹, Liwang Ren¹, Jia Li², Lingan Kong¹, Yujia Zeng¹, Quanyang Tao¹, Ruixia Wu², Huifang Ma², Bei Zhao², Di Wang², Weiqi Dang², Keqiu Chen¹ , Lei Liao¹ , Xidong Duan², Xiangfeng Duan³  & Yuan Liu¹ 

Strain engineering is a promising method to manipulate the electronic and optical properties of two-dimensional (2D) materials. However, with weak van der Waals interaction, severe slippage between 2D material and substrate could dominate the bending or stretching processes, leading to inefficiency strain transfer. To overcome this limitation, we report a simple strain engineering method by encapsulating the monolayer 2D material in the flexible PVA substrate through spin-coating approach. The strong interaction force between spin-coated PVA and 2D material ensures the mechanical strain can be effectively transferred with negligible slippage or decoupling. By applying uniaxial strain to monolayer MoS₂, we observe a higher bandgap modulation up to ~300 meV and a highest modulation rate of ~136 meV/%, which is approximate two times improvement compared to previous results achieved. Moreover, this simple strategy could be well extended to other 2D materials such as WS₂ or WSe₂, leading to enhanced bandgap modulation.

¹Key Laboratory for Micro-Nano Optoelectronic Devices of Ministry of Education, School of Physics and Electronics, Hunan University, Changsha 410082, China. ²State Key Laboratory for Chemo/Biosensing and Chemometrics, College of Chemistry and Chemical Engineering, Hunan University, Changsha 410082, China. ³Department of Chemistry and Biochemistry, University of California, Los Angeles, CA 90095, USA. ✉email: yuanliuhnu@hnu.edu.cn

The two-dimensional (2D) materials have attracted considerable attention in recent years, owing to their unique electrical, optical, and mechanical properties at the single atomic thickness^{1–8}. From mechanical point of view, 2D materials could withstand deformations over 10% before rupture, which is over one order of magnitude higher than that of typical bulk semiconductors with a break value typically <1% (refs. 7,9). The naturally high flexibility has stimulated considerable efforts in further controlling and modulating the electrical and optical properties of 2D semiconductors through strain engineering. For example, by applying tension strains, the bandgap of typical TMD (transition metal dichalcogenide) can be reduced, offering additional degree of freedom to improve the performance of TMD based devices such as strain-induced strong light emission in bilayer WSe₂ (ref. 10), and the greatly enhanced carrier mobilities in strained MoS₂ transistors^{11,12}.

In modern microelectronics, the strain engineering of silicon channel is achieved by doping the source and drain regions with lattice-mismatched atoms such as germanium and carbon¹³. The larger germanium atom provides compression strain to silicon channel with much-enhanced hole carrier mobility, and similarly, smaller carbon atom creates tension strain and is used to increase the electron carrier mobility of silicon. Applying existing state-of-the-art strain approaches to 2D materials is not straightforward because there is little physical space for impurity dopants in such atomically thin semiconductors¹⁴. Alternatively, in 2D research community, the strain engineering is typically achieved by mechanically exfoliating 2D materials on the surface of flexible polymer substrate that can be mechanically bended or stretched^{10,15–19}. However, with weak van der Waals (vdW) force in between²⁰, the strain applied on the polymer may not be effectively transferred to the lattice of 2D materials where the decoupling (between polymer and 2D materials) and interlayer slippage are unavoidable¹⁸, leading to insufficient bandgap modulation. For example, by applying uniaxial strain to monolayer MoS₂ on PMMA (polymethyl methacrylate) substrate, small bandgap change (ΔE_g) of 38 meV and low bandgap modulation rate ($S_{\Delta E_g}$, defined as the slope between ΔE_g and applied strain) ~70 meV/% are observed²¹.

To enhance the ΔE_g and $S_{\Delta E_g}$, considerable efforts have been devoted to increase the strain transfer efficiency from polymer substrate to 2D materials. The early attempt used Ti metal as a clamp to fix the MoS₂ on the surface of flexible PET (polyethylene terephthalate) substrate to avoid the slippage²². However, within this structure, the majority strain may be largely accumulated in the metal–MoS₂ junction, resulting in nonhomogeneous strain distribution and small bandgap modulation ΔE_g of 110 meV (with $S_{\Delta E_g}$ ~ 45 meV/%) before MoS₂ rupture. Alternatively, improved strain transfer efficiency can be achieved by using polymers with higher Young's modulus E_{Young} , which have been theoretically predicted and experimentally verified^{23,24}. For example, by changing the flexible substrate from polydimethylsiloxane (PDMS) (E_{Young} ~ 430 kPa) to polyvinyl alcohol (PVA) (E_{Young} ~ 650 MPa), the strain transfer efficiency could be improved over 6 fold¹⁸. However, although increasing the substrate E_{Young} could mitigate the Young's modulus mismatch between 2D materials and substrate, their vdW interaction is still too weak to prevent slippage and interfacial decoupling during straining process, especially at relatively large strain level. Hence using uniaxial strain, the highest bandgap modulation reported for monolayer MoS₂, WSe₂, and WS₂ are limited to 140 meV, 90 meV, 50 meV, respectively^{18,25}. The non-optimized bandgap modulation achieved poses a key challenge for investigating fundamental physics of 2D materials through strain engineering, as well as for the practical application of high-performance strain engineered 2D devices and flexible electronics.

Here, we report a simple strain engineering approach to efficiently modulate the bandgap of 2D materials, by encapsulating them in the flexible PVA through spin-coating method. The strong interaction force between the spin-coated PVA and 2D materials, together with the high Young's modulus of PVA used here (E_{Young} ~ 10 GPa)²⁶, ensure the mechanical strain applied on the PVA substrate can be effectively transferred to the lattice of 2D materials during the mechanical bending process. By applying uniaxial strain to monolayer MoS₂, we observed a higher bandgap change of ~300 meV and a highest modulation rate of ~136 meV/%, approximate two times improvement compared to previous best results (ΔE_g ~ 140 meV and $S_{\Delta E_g}$ ~ 70 meV/%, respectively) using uniaxial strain and is approaching the energy required for direct-to-indirect bandgap transition in MoS₂ (refs. 18,21). Furthermore, tape peeling test, thermal expansion measurement, multiple cycles straining-relaxing, and load-unload experiments are conducted to verify the efficient bandgap modulation is the result of strong interaction between MoS₂ and PVA substrate with negligible slippage in between. Finally, we demonstrate this simple PVA spin-coating approach could be well extended to other TMD such as WS₂ or WSe₂, and much higher ΔE_g and $S_{\Delta E_g}$ are observed compared to previous reports. Our study not only breaks the limit of TMD bandgap modulation value using strain engineering, but also provides a general approach for efficient strain engineering of other layered 2D materials and conventional 3D thin films.

Results

Device fabrication and straining processes. Figure 1 shows the schematic fabrication processes and device structure. To fabricate the device, monolayer MoS₂ is first mechanically exfoliated on the surface of silicon substrate (p⁺⁺) with 300 nm SiO₂ on top (Fig. 1a, i). The monolayer thickness of MoS₂ used here can be confirmed by optical micrograph, Raman spectrum and photoluminescence (PL) spectrum, as shown in Supplementary Fig. 1. Next, PVA layer (with a thickness of ~13 μm) is spin-coated on top of substrate, and fully encapsulates the MoS₂ underneath, as shown in Fig. 1a, ii. The spin-coated PVA used here could provide strong bonding forces towards underneath MoS₂ (highlighted by the red links in Fig. 1a), which is essential for efficient strain transfer and will be discussed in detail. After fully encapsulating the MoS₂ underneath, the PVA and the MoS₂ are physically released from the SiO₂ substrate and fixed on two-point apparatus that could continuously apply strain through bending process (Fig. 1a, iii) under a Raman system. When the device is bended, uniaxial tension strain applied on the PVA will be efficiently transferred onto MoS₂ with negligible slippage owing to their strong interaction, as schematically illustrated in Fig. 1a, iv. The details of apparatus setup and the measurement of strain value are shown in the “Method” section and Supplementary Fig. 2. For comparison, the fabrication processes of control device using conventional direct exfoliation method is also schematically illustrated. As shown in Fig. 1b, i, the monolayer MoS₂ is mechanically exfoliated on top of pre-fabricated PVA substrate (with same substrate preparation condition as in Fig. 1a), demonstrating low vdW bonding forces towards the PVA substrate. When the strain is applied through mechanically bending, large slippage could happen, as highlighted by the distance between the red dash line (ideal position without slippage) and the blue dash line (actual 2D material edge) in Fig. 1b, ii. The device structures fabricated through both spin-coated encapsulation method and conventional exfoliation method can be further confirmed using atomic force microscopy, as shown in Supplementary Fig. 3.

Bandgap modulation of monolayer MoS₂ under uniaxial strain. We investigate the evolution of the band structure of monolayer MoS₂ under uniaxial strain through PL and Raman

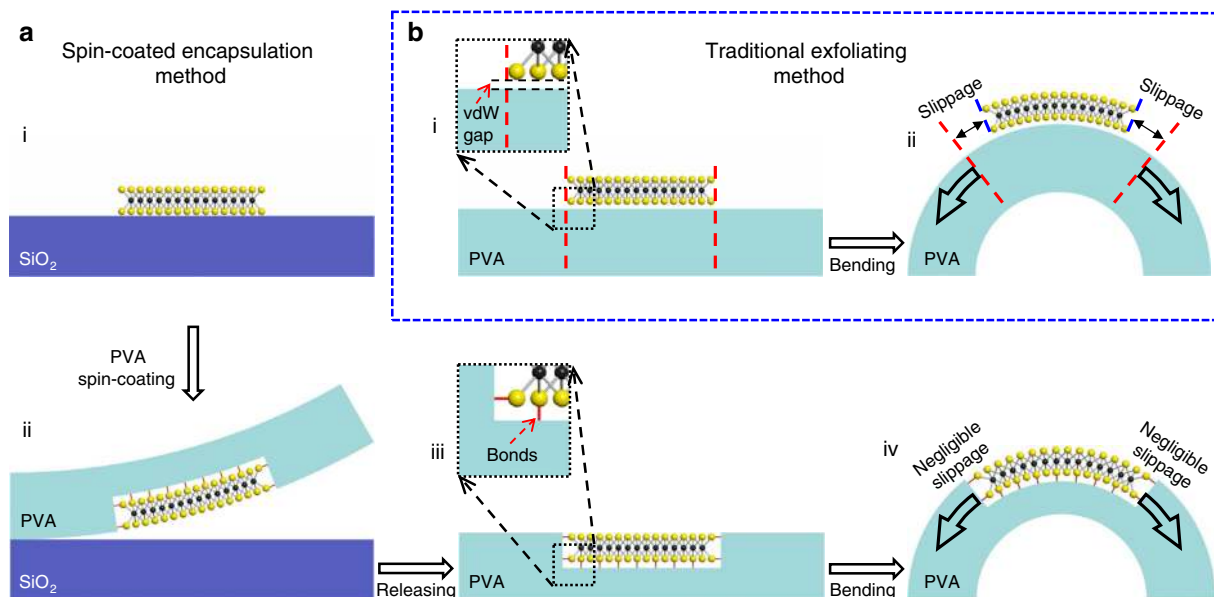


Fig. 1 Schematic illustration of fabrication processes of spin-coated encapsulation method and traditional exfoliating method. **a** Schematic fabrication processes of PVA-encapsulation method with four steps: (i) MoS₂ exfoliation on SiO₂ substrate, (ii) PVA spin-coating and fully encapsulation of MoS₂ with strong interaction force in between, (iii) PVA/MoS₂ released from SiO₂ substrate, (iv) bended under strain test equipment with negligible slippage. **b** Schematic fabrication processes of traditional exfoliating method with two steps: (i) MoS₂ direct exfoliation on top of the pre-fabricated PVA substrate, (ii) bended under strain test equipment. Due to the weak vdW force between PVA and MoS₂, large slippage could happen under tension strain, as highlighted by the distance between the red dash line (ideal position without slippage) and the blue dash line (actual 2D material edge with slippage).

measurement. As shown in Fig. 2a–c, the spectra of the unstrained PVA-encapsulated MoS₂ shows a prominent A peak at 1.883 eV, suggesting its direct bandgap. Applying tension strain significantly decreases its bandgap (Fig. 2b), and with the strain level of 1.49%, the PL peak value red shifts from 1.883 to 1.690 eV with a ΔE_g of 193 meV, much higher than that previously achieved in monolayer MoS₂ ($\Delta E_g \sim 140$ meV). The relationship between peak position and the strain value is summarized in Fig. 2c, and the linear fitted strain modulation rate $S_{\Delta E_g}$ reaches 125 meV/%, which is consistent with 136 meV/% of our density functional theory (DFT) simulation and the previous simulation results^{27,28}, as detailed in Supplementary Fig. 4. We note that with further increasing the applying strain value above 1.7%, the strong interaction between MoS₂ and the substrate may eventually break, leading to the strain relaxation and the device failure, as schematically illustrated and experimentally demonstrated in Supplementary Fig. 5.

Besides the peak position, the peak intensity also reduces with increasing strain, owing to the direct-to-indirect band transition with applying tension strain²². Moreover, in order to probe the limit of bandgap modulation and strain tuning capability, we also measure the PL spectrum of the device under compression strain, where highest $\Delta E_g \sim 300$ meV and $S_{\Delta E_g} \sim 136$ meV/% are demonstrated, as shown in Supplementary Fig. 6. Besides PL measurement, Raman spectrum is also measured to investigate the lattice change of MoS₂ device under strain, as shown in Fig. 2d. With the strain value increasing, the A' peak (out-of-plane vibration) keeps relatively constant, and the E' peak (in-plane vibration) redshift towards lower wavenumber, which is expected and consistent with the previous reports²². Importantly, as the lattice symmetry is gradually broken, we observe a pronounced E' peak split behavior (into E'⁻ and E'⁺, as shown in Fig. 2d), further indicating the applied strain is efficiently transferred to MoS₂ lattice. When the strain reaches 1.49%, the E'⁻ peak shows a maximum red shift of 11.1 cm⁻¹ with an average slope of about 7.4 cm⁻¹/% strain, which is also much higher than previous reports (4.5 cm⁻¹/% or 2.1 cm⁻¹/%)^{22,29}.

To highlight the efficiency of our PVA-encapsulation method, the same bending and spectrums measurements are also applied to our control sample with conventional strain engineering approach, by exfoliating monolayer MoS₂ on top of pre-fabricated PVA substrate (Figs. 1b and 2e). As shown in Fig. 2f, g, the exfoliated MoS₂ demonstrate expected bandgap reduction with applying tension strain. However, due to the weak vdW force between MoS₂ and the substrate, the strain can not be fully transferred to the lattice of MoS₂. Hence, small $\Delta E_g \sim 90$ meV, $S_{\Delta E_g} \sim 61$ meV/% and Raman shift slope ~ 3.2 cm⁻¹/% strain are observed under the same strain level (1.49%), both of which are less than half of the PVA-encapsulated samples and are consistent with previous reports^{18,22}, further suggesting the decoupling between sample and substrate, as well as the inefficient strain transfer using conventional approach. We note the slippage or decoupling effect may not only exist in uniaxial experiment (through substrate bending), but could also happen for biaxial straining of 2D materials using AFM tip based or micro-chamber based blister or balloon experiments owing to the weak vdW interaction between 2D material and the anchor substrate during the chamber pressure change, as have been reported in previous literatures^{30–32}.

Furthermore, the demonstrated effective strain modulation is a robust behavior within different locations of given sample, as well as between different samples. To demonstrate this, we have applied PL mapping to monolayer MoS₂ samples fabricated through both our spin-coated encapsulation method, as well as conventional exfoliation approach. As shown in Supplementary Fig. 7, for conventional exfoliation sample with weak MoS₂–PVA interaction, the PL peaks show visible peak fluctuation (~ 30 meV), consistent with previous literature¹⁶ and the highest bandgap modulation is ~ 60 meV under strain of 1.28%. In contrast, the device fabricated through our PVA encapsulation approach shows more uniform PL peak (with negligible variation) and the bandgap modulation value is ~ 120 meV, which is around two times improvement compared to conventional exfoliation method. Furthermore, we have also measured multiple devices to

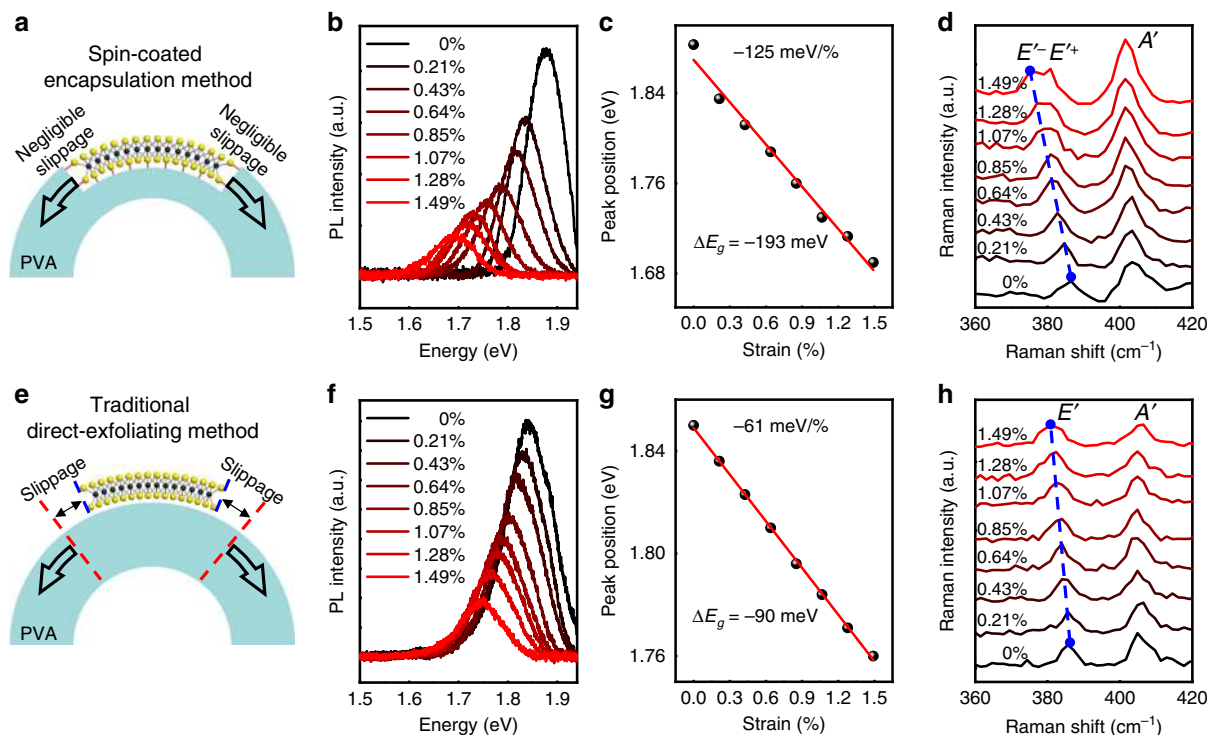


Fig. 2 Bandgap modulation of monolayer MoS₂ using uniaxial tension strain. **a–d** PL and Raman spectrums under different mechanical strain using spin-coated PVA encapsulation method. **b** PL spectrum under different tension strain. **c** With applying tension strain up to 1.49%, large bandgap modulation ΔE_g of -193 meV is observed with a highest modulation efficiency of 125 meV/% using linear fitting (red line). **d** Raman spectrum under different tension strain, and the E' peak shows a red shift of 11.1 cm⁻¹ with an average slope of about 7.4 cm⁻¹/% strain when strain value reaches 1.49%. **e–h** PL and Raman spectrums under different mechanical strain using the traditional direct exfoliating method. **f** PL spectrum under different tension strain. **g** With tension strain up to 1.49%, bandgap modulation ΔE_g of -90 meV is observed with a modulation efficiency of 61 meV/% using linear fitting (red line). The much smaller ΔE_g and slope suggest the inefficient strain transfer from substrate to MoS₂ using conventional exfoliation approach. **h** Raman spectrum under different tension strain, and the E' peak shows a red shift of 4.8 cm⁻¹ with an average slope of about 3.2 cm⁻¹/% strain when strain value reaches 1.49%.

show the consistency of our data, and to produce the confidence interval for the measured parameters. As shown in Supplementary Fig. 8, for our spin-coating encapsulation method, the maximum modulation value is in the range of 190 meV to 240 meV using tension strain, and the modulation efficiency is in the range of 125 meV/% to 131 meV/%. In contrast, for devices using conventional exfoliation approach, the maximum modulation value is in the range of 90 meV to 110 meV, and the modulation efficiency is in the range of 44 meV/% to 63 meV/%.

Mechanisms of the efficient strain transfer. The efficient bandgap modulation achieved above could be attributed to three advantages of our PVA encapsulation method. First, the most functional groups of PVA are hydroxyl groups³³, and therefore could provide a stronger adhesion force towards the MoS₂ than typical PDMS or PET substrate used. In fact, PVA itself has been widely used as adhesive glue in the textile industry owing to its excellent adhesion properties^{34,35}. Secondly, the spin-coating method ensures the conformal contact between PVA and MoS₂ and the possible chemical bonds at the defects points and edge sidewall of MoS₂ (as highlighted in Fig. 1a, iii), which is much stronger compared to the conventional approaches with weak vdW bonding forces^{33,36}. It has been reported that the sulfur vacancy³⁷ is the primary defect of MoS₂ and the defect density could reach as high as $6.5 \times 10^{13}/\text{cm}^2$, which would provide enough dangling-bonds to form strong interaction with spin-coated PVA. To confirm this, we have further applied tape peeling test, as shown in Supplementary Fig. 9. For convention MoS₂ exfoliated on top of pre-fabricated PVA substrate with

weak vdW interaction, there is no sample left on PVA anymore after peeling by tapes (Supplementary Fig. 9c, f). In great contrast, MoS₂ flakes encapsulated in PVA can pass this peeling test and remains on PVA substrate after repeated peeling using different tapes (Supplementary Fig. 9h–k), suggesting stronger interaction force between MoS₂ and PVA (compared to that of MoS₂ and tapes). Thirdly, the PVA used here have a larger $E_{\text{Young}} \sim 10$ GPa, which is much higher than typical used PDMS with E_{Young} of 430 KPa. The high E_{Young} here is essential for efficient strain transfer to MoS₂, as have been theoretically analyzed using finite element simulation (Supplementary Fig. 10) and experimentally demonstrated in our samples with different substrate E_{Young} (Supplementary Fig. 11). Together with strong interaction force (to hold PVA and MoS₂) and high substrate E_{Young} , the simple spin-coated PVA encapsulation method used here could provide near unity strain transfer efficiency, as can also be quantitatively and directly measured using optical microscope through thermal expansion experiment (Supplementary Fig. 12).

Multi-cycles load and unload test. To further confirm the high strain transfer efficiency and negligible material slippage, multiple cycles straining-relaxing test is conducted. Figure 3a, b show the extracted PL peak position as a function of the repeated cycles of straining and relaxing, and strain value is fixed at 1.28%. For our PVA-encapsulated sample, the PL emission peak always comes back to the same value between each cycle, indicating that the MoS₂ flake does not slip during the measurement and the applied strain is successfully transferred to the lattice of MoS₂, as highlighted by the blue dash line (Fig. 3a). In great contrast, the

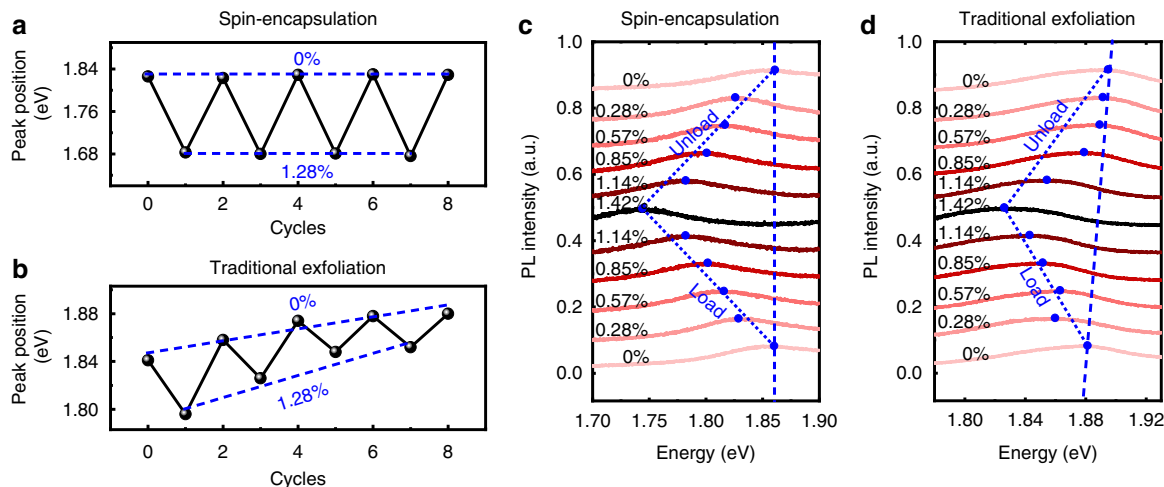


Fig. 3 Multiple cycles straining-relaxing and load-unload bending test. **a, b** The multiple cycles straining and relaxing at fixed tension strain of 1.28%, for devices fabricated by our PVA encapsulation method (**a**) and the conventional exfoliating approach (**b**). Within spin-coated PVA approach (**a**), the PL spectrums demonstrate repeatable peak position under multiple cycles test, suggesting the negligible slippage and efficient strain transfer. In contrast, within conventional exfoliating approach (**b**), the PL spectrums demonstrate a much smaller ΔE_g and a gradual blue shift with increasing bending cycles, indicating the poor strain transfer and a significant slippage behavior. **c, d** The load-unload bending test under variable tension strain level, for our PVA encapsulation method (**c**) and the conventional exfoliating approach (**d**). Within spin-coated PVA approach (**c**), the PL spectrums demonstrate repeatable peak position change, further confirming the negligible slippage and efficient strain transfer. In contrast, within conventional exfoliating approach (**d**), the PL spectrums demonstrate much smaller modulation efficiency and blue shift of peak position during unloading process, indicating that the poor strain transfer and a significant slippage behavior.

control sample of exfoliated MoS₂ (on pre-fabricated PVA substrate) shows much smaller ΔE_g with applying same level of strain, as shown in Fig. 3b. More importantly, with increasing the straining-relaxing cycles, the PL peak of control sample gradually blueshift and can not back to the same value between each cycle (highlighted by the blue dash line in Fig. 3b), indicating the material slippage and the substrate decoupling dominate the whole bending process. Such small non-repeatable PL spectrum (within weakly bonded system) have also been observed in previous studies^{24,38}, which may be attributed to the finite in-plane compression during the unloading process, as shown in Supplementary Fig. 13.

Furthermore, the minimized material slippage can also be confirmed by load-unload test, where continuous strain is applied and withdrawn from the sample. As shown in Fig. 3c, d, for our spin-coated encapsulation sample, the unloading process shows identical PL spectrums with the loading process (Fig. 3c, blue dash line), where the PL peak can go back to its original value under different strain level. In contrast, for direct exfoliated control sample, very small bandgap changes, and non-repeatable PL spectrums are observed, further confirming the MoS₂ slippage and inefficient strain transfer during bending process.

Bandgap modulation for a variety of other monolayer 2D materials. The simple spin-coated PVA encapsulation approach is not only limited to MoS₂, but could be well-extended to other 2D semiconductors to achieve higher bandgap modulation than typical exfoliation approach. To demonstrate this, we have applied this simple method to mechanically exfoliated monolayer WSe₂, CVD (chemical vapor deposition) grown monolayer WSe₂, as well as CVD grown monolayer WS₂. As shown in Fig. 4a–f, all of these materials demonstrate distinct bandgap reduction with applying uniaxial tension strain, consistent with MoS₂ and previous reports. The peak position can be further extracted and plotted as a function of the strain applied. As shown in Fig. 4b, d, f, highest ΔE_g of 176 meV ($S_{\Delta E_g} = 109$ meV/%), 137 meV ($S_{\Delta E_g} = 53$ meV/%), 253 meV ($S_{\Delta E_g} = 43$ meV/%) are observed for exfoliated WSe₂,

CVD WSe₂, and CVD WS₂, respectively. The difference between exfoliated WSe₂ and CVD grown WSe₂ could be attributed to the inferior quality of CVD grown samples, with possible dopants, defects, or pre-strains. Nevertheless, the observed ΔE_g values are much higher than previous reports^{10,16,18,21,22,25,39–44}, indicating our method is a general approach for effective strain transfer with negligible slippage.

At last, we compare the performance of our PVA-encapsulation approach with previous strain engineering methods in terms of ΔE_g and $S_{\Delta E_g}$. As shown in Fig. 4g, our spin-coated PVA encapsulation approach demonstrates higher ΔE_g and $S_{\Delta E_g}$, as highlighted by blue area, and is much higher than various strain engineering methods in previous reports (highlighted by the gray area). This suggests that our simple strain engineering approach may be further extended to other emerging 2D materials or thin film semiconductors, with another degree of freedom to further manipulate their band structures, as well as electronic transport properties (e.g., high mobilities in Hall bar structure, or lower contact resistance in transistor). Furthermore, we note the efficient straining of vdW heterostructures would be an interesting topic for future investigation. However, our spin-coating encapsulation method only provide strong interaction between the PVA substrate and one layer of 2D material, while the heterostructures are still bonded through weak vdW interaction and the interlayer slippage may dominate the overall device straining behavior.

Discussion

In summary, we report a simple and efficient strain engineering approach to modulate the bandgap of monolayer 2D materials by using PVA encapsulation through a spin-coating method. The strong adhesion force (between the spin-coated PVA and 2D materials) and high $E_{Y_{\text{oung}}}$ of PVA ensure the mechanical strain can be effectively transferred to the lattice of 2D materials. By applying uniaxial strain to monolayer MoS₂, we observed a higher bandgap modulation $\Delta E_g \sim 300$ meV and $S_{\Delta E_g} \sim 136$ meV/%, which is approximately two times enhancement compared to previous best

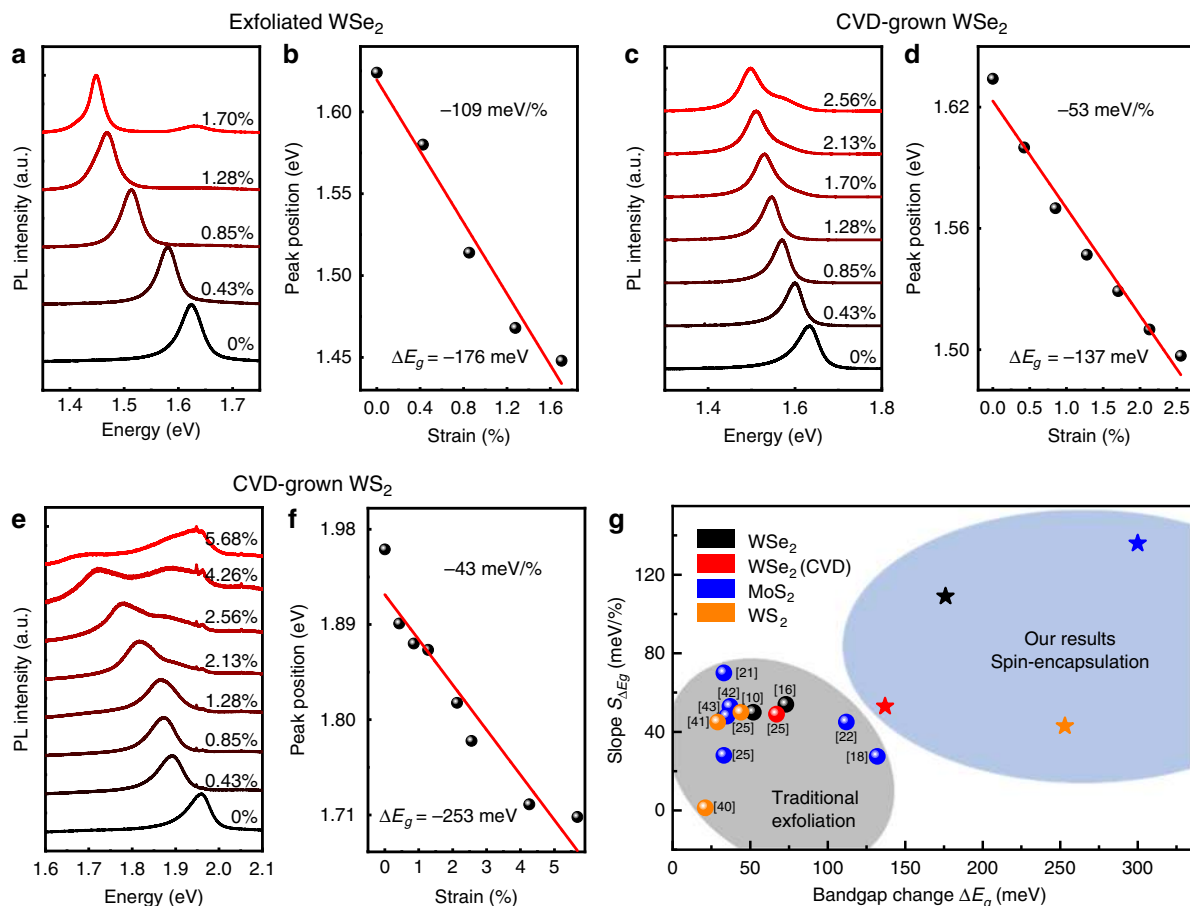


Fig. 4 Photoluminescence measurement under different tension strain of other TMD materials using PVA encapsulation approach. **a, b** PL spectrum of mechanically exfoliated monolayer WSe_2 under difference strain (**a**). The bandgap change ΔE_g is 176 meV with a linear fitted slope of 109 meV/% (**b**). **c, d** PL spectrum of the monolayer CVD-grown WSe_2 under difference strain (**c**). The bandgap change ΔE_g is 137 meV with a linear fitted slope of 53 meV/% (**d**). **e, f** PL spectrum of monolayer CVD-grown WS_2 under difference strain (**e**). The bandgap change ΔE_g is 253 meV with a linear fitted slope of 43 meV/% (**f**). **g** The bandgap strain modulation of different materials and different approaches. Our spin-encapsulation method (highlighted by blue area) provides higher ΔE_g (x-axis) and $S_{\Delta E_g}$ (y-axis), compared to that of the traditional exfoliation method (highlighted by gray area).

results, and is consistent with our DFT calculations. Furthermore, we confirmed the negligible slippage (between TMD and spin-coated PVA) in our system through detailed tape peeling test, multiple cycles straining-relaxing, thermal expansion measurement, and load-unload bending experiments. Our simple method offers a general strain engineering approach beyond the limit conventional direct-exfoliating method, providing another degree-of-freedom to discover and to investigate the fundamental physics in 2D layered materials as well as conventional 3D thin film materials. It may also provide exciting implications for electronic, optoelectronics, nanoelectromechanical systems, and other devices that can benefit from the flexible, transparent nature of atomic monolayers.

Methods

PVA substrate preparation. For PVA encapsulation method, monolayer MoS_2 is first mechanically exfoliated on the surface of the silicon substrate (p^{++}) with 300 nm SiO_2 on top (substrate size: $30 \times 10 \text{ mm}^2$). Next, 10 wt% PVA (Alfa Aesar, 98–99% hydrolyzed, molecular weight 130,000 g/mol) solution is spin-coated on the surface of SiO_2 (with MoS_2) at a speed of 1000 rpm for 40 s, and baked at 70°C (1 min) to remove water solvent. Subsequently, a PET (Shanghai Feixia Rubber and Plastic Hardware Trading Co., Ltd, 125 μm thick) film is glued onto the upper surface of the PVA film using adhesive glue (Shenzhen Kaibingtuan Plastic Industry Co., Ltd, 5562 instant adhesive) to increase the thickness for easily handling of flexible substrate. Next, the entire flexible substrate (PVA/glue/PET) with the encapsulated MoS_2 can be slowly peeled off from SiO_2 substrate using tweezers, as shown in the Fig. 1a, ii. The PVA film prepared here is measured to be $\sim 13 \mu\text{m}$ and entire flexible substrate is measured to be $\sim 185 \mu\text{m}$ (PVA/glue/PET), as shown in the schematic and cross-section optical image in Supplementary Fig. 2a, b.

Calculation of tension strain values. In general, the strain applied on flexible substrate can be expressed through the simple equation $\epsilon = \tau/R$, where 2τ and R are the substrate thickness and curvature radius, respectively. The thickness 2τ of the entire flexible substrate is accurately measured to be $\sim 185 \mu\text{m}$ through the cross-section optical image, as shown in Supplementary Fig. 2a, b. Therefore, the measurement of bending curvature is the key factor for the substrate strain calculation. To accurately measure the actual curvature radius R , we have imaged the curvature radius through both the cross-sectional optical image and photograph, and directly measured the accurate curvature radius R under the device, as shown red dash line in Supplementary Fig. 2c–e (fitted using commercial software Digimizer).

First-principles calculations. The first-principles calculation is carried out by the open-source QUANTUM ESPRESSO plane-wave density functional theory (DFT) package^{45,46}. The Perdew-Burke-Ernzerhof (PBE) exchange-correlation functional with semi-empirical DFT-D3 vdW correction method is adopted⁴⁷ and the plane-wave cut-off energy is 1115 eV. To avoid mirror interactions, a vacuum space of 15 \AA is added between adjacent cells in the thickness direction. The Brillouin zone k -point sampling is $10 \times 10 \times 1$ for electronic ground-state computations. The crystal structures are fully relaxed until the force on each atom and total energy variations are smaller than $2.6 \times 10^{-2} \text{ eV}/\text{\AA}$ and $1.4 \times 10^{-3} \text{ eV}$ (ref. 48). The strains are achieved by varying the relaxed cell parameters and the atom positions are optimized again after the variations.

3D finite element (FE) simulation. The discretized FE models contain about 12,099 units with very fine meshes in the contact region. The final mesh density was determined through a series of convergence studies. Appropriate boundary conditions were used along two edges of the PVA to simulate the loading strain. The interface between MoS_2 and PVA were modeled using perfect bonding. The calculations were performed using commercial FE package COMSOL

Multiphysics (version 5.2). Young's modulus and Poisson's ratio are 10 GPa and 0.3 for PVA substrate, 170 GPa and 0.27 for MoS₂ nanosheet, respectively.

Raman and PL measurement. The entire mechanical device and flexible substrate are placed on a confocal microscope (Renishaw inVia-reflex) to measure Raman and photoluminescence spectrums. For PL spectrum measurement, 532 nm laser with 1800 lines mm⁻¹ grating is used, where laser power is 500 μW (MoS₂), 50 μW (WS₂) and 500 μW (WS₂), respectively. For Raman spectrum measurement, 488 nm laser is used with 250 μW power and a grating levels of 2400 lines mm⁻¹.

Data availability

The data that support the findings of this study are available from the corresponding author upon reasonable request.

Received: 7 July 2019; Accepted: 14 February 2020;

Published online: 02 March 2020

References

- Novoselov, K. S. et al. Two-dimensional atomic crystals. *Proc. Natl Acad. Sci. USA* **102**, 10451–10453 (2005).
- El-Bana, M. S. et al. Superconductivity in two-dimensional NbSe₂ field effect transistors. *Supercond. Sci. Technol.* **26**, 125020 (2013).
- Butler, S. Z. et al. Progress, challenges, and opportunities in two-dimensional materials beyond graphene. *ACS Nano* **7**, 2898–2926 (2013).
- Castellanos-Gomez, A., Agrait, N. & Rubio-Bollinger, G. Optical identification of atomically thin dichalcogenide crystals. *Appl. Phys. Lett.* **96**, 213116 (2010).
- Xu, M., Liang, T., Shi, M. & Chen, H. Graphene-like two-dimensional materials. *Chem. Rev.* **113**, 3766–3798 (2013).
- Castellanos-Gomez, A. et al. Fast and reliable identification of atomically thin layers of TaSe₂ crystals. *Nano Res.* **6**, 191–199 (2013).
- Bertolazzi, S., Brivio, J. & Kis, A. Stretching and breaking of ultrathin MoS₂. *ACS Nano* **5**, 9703–9709 (2011).
- Zeng, Y. J. et al. Nanoscale organic thermoelectric materials: measurement, theoretical models, and optimization strategies. *Adv. Funct. Mater.* <https://doi.org/10.1002/adfm.201903873> (2019).
- Feng, J., Qian, X., Huang, C.-W. & Li, J. Strain-engineered artificial atom as a broad-spectrum solar energy funnel. *Nat. Photonics* **6**, 866–872 (2012).
- Desai, S. B. et al. Strain-induced indirect to direct bandgap transition in multilayer WSe₂. *Nano Lett.* **14**, 4592–4597 (2014).
- Hosseini, M., Elahi, M., Pourfath, M. & Esseni, D. Strain induced mobility modulation in single-layer MoS₂. *J. Phys. D: Appl. Phys.* **48**, 375104 (2015).
- Yu, S., Xiong, H. D., Eshun, K., Yuan, H. & Li, Q. Phase transition, effective mass and carrier mobility of MoS₂ monolayer under tensile strain. *Appl. Surf. Sci.* **325**, 27–32 (2015).
- Ang, K.-W. et al. Lattice strain analysis of transistor structures with silicon–germanium and silicon–carbon source/drain stressors. *Appl. Phys. Lett.* **86**, 093102 (2005).
- Allain, A., Kang, J., Banerjee, K. & Kis, A. Electrical contacts to two-dimensional semiconductors. *Nat. Mater.* **14**, 1195–1205 (2015).
- Castellanos-Gomez, A. et al. Local strain engineering in atomically thin MoS₂. *Nano Lett.* **13**, 5361–5366 (2013).
- Schmidt, R. et al. Reversible uniaxial strain tuning in atomically thin WSe₂. *2D Mater.* **3**, 021011 (2016).
- Island, J. O. et al. Precise and reversible band gap tuning in single-layer MoSe₂ by uniaxial strain. *Nanoscale* **8**, 2589–2593 (2016).
- Liu, Z. et al. Strain and structure heterogeneity in MoS₂ atomic layers grown by chemical vapour deposition. *Nat. Commun.* **5**, 5246 (2014).
- Shen, T., Penumatcha, A. V. & Appenzeller, J. Strain engineering for transition metal dichalcogenides based field effect transistors. *ACS Nano* **10**, 4712–4718 (2016).
- Liu, Y., Huang, Y. & Duan, X. Van der Waals integration before and beyond two-dimensional materials. *Nature* **567**, 323–333 (2019).
- He, K., Poole, C., Mak, K. F. & Shan, J. Experimental demonstration of continuous electronic structure tuning via strain in atomically thin MoS₂. *Nano Lett.* **13**, 2931–2936 (2013).
- Conley, H. J. et al. Bandgap engineering of strained monolayer and bilayer MoS₂. *Nano Lett.* **13**, 3626–3630 (2013).
- Frisenda, R. et al. Biaxial strain tuning of the optical properties of single-layer transition metal dichalcogenides. *npj 2D Mater. Appl.* **1**, 10 (2017).
- Gong, L. et al. Interfacial stress transfer in a graphene monolayer nanocomposite. *Adv. Mater.* **22**, 2694–2697 (2010).
- Niehues, I. et al. Strain control of exciton-phonon coupling in atomically thin semiconductors. *Nano Lett.* **18**, 1751–1757 (2018).
- Peng, J., Ellingham, T., Sabo, R., Turng, L.-S. & Clemons, C. M. Short cellulose nanofibrils as reinforcement in polyvinyl alcohol fiber. *Cellulose* **21**, 4287–4298 (2014).
- Lu, P., Wu, X., Guo, W. & Zeng, X. C. Strain-dependent electronic and magnetic properties of MoS₂ monolayer, bilayer, nanoribbons and nanotubes. *Phys. Chem. Chem. Phys.* **14**, 13035–13040 (2012).
- Johari, P. & Shenoy, V. B. Tuning the electronic properties of semiconducting transition metal dichalcogenides by applying mechanical strains. *ACS Nano* **6**, 5449–5456 (2012).
- Rice, C. et al. Raman-scattering measurements and first-principles calculations of strain-induced phonon shifts in monolayer MoS₂. *Phys. Rev. B* **87**, 081307 (2013).
- Kitt, A. L. et al. How graphene slides: measurement and theory of strain-dependent frictional forces between graphene and SiO₂. *Nano Lett.* **13**, 2605–2610 (2013).
- Lloyd, D. et al. Band gap engineering with ultralarge biaxial strains in suspended monolayer MoS₂. *Nano Lett.* **16**, 5836–5841 (2016).
- Wang, G. et al. Measuring interlayer shear stress in bilayer graphene. *Phys. Rev. Lett.* **119**, 036101 (2017).
- Park, H.-K., Kong, B.-S. & Oh, E.-S. Effect of high adhesive polyvinyl alcohol binder on the anodes of lithium ion batteries. *Electrochem. Commun.* **13**, 1051–1053 (2011).
- Zhu, Z. & Qian, K. Effects of the molecular structure of polyvinyl alcohol on the adhesion to fibre substrates. *Fibres Text. East. Eur.* **15**, 82–85 (2007).
- Gaaz, T. S. et al. Properties and applications of polyvinyl alcohol, halloysite nanotubes and their nanocomposites. *Molecules* **20**, 22833–22847 (2015).
- Sin, L. T., Rahman, W. A. W. A., Rahmat, A. R. & Samad, A. A. Computational modeling and experimental infrared spectroscopy of hydrogen bonding interactions in polyvinyl alcohol–starch blends. *Polymer* **51**, 1206–1211 (2010).
- Yu, Z. et al. Towards intrinsic charge transport in monolayer molybdenum disulfide by defect and interface engineering. *Nat. Commun.* **5**, 5290 (2014).
- Jiang, T., Huang, R. & Zhu, Y. Interfacial sliding and buckling of monolayer graphene on a stretchable substrate. *Adv. Funct. Mater.* **24**, 396–402 (2014).
- Wu, W. et al. Giant mechano-optoelectronic effect in an atomically thin semiconductor. *Nano Lett.* **18**, 2351–2357 (2018).
- Zhang, Q. et al. Strain relaxation of monolayer WS₂ on plastic substrate. *Adv. Funct. Mater.* **26**, 8707–8714 (2016).
- He, X. et al. Strain engineering in monolayer WS₂, MoS₂, and the WS₂/MoS₂ heterostructure. *Appl. Phys. Lett.* **109**, 173105 (2016).
- Pak, S. et al. Strain-mediated interlayer coupling effects on the excitonic behaviors in an epitaxially grown MoS₂/WS₂ van der Waals heterobilayer. *Nano Lett.* **17**, 5634–5640 (2017).
- Zhu, C. R. et al. Strain tuning of optical emission energy and polarization in monolayer and bilayer MoS₂. *Phys. Rev. B* **88**, 121301 (2013).
- Hui, Y. Y. et al. Exceptional tunability of band energy in a compressively strained trilayer MoS₂ sheet. *ACS Nano* **7**, 7126–7131 (2013).
- Giannozzi, P. et al. Quantum espresso: a modular and open-source software project for quantum simulations of materials. *J. Phys.: Condens. Matter* **21**, 395502 (2009).
- Islamov, D. R. & Perevalov, T. V. Effect of oxygen vacancies on the ferroelectric Hf_{0.5}Zr_{0.5}O₂ stabilization: DFT simulation. *Microelectron. Eng.* **216**, 111041 (2019).
- Liu, Y., Merinov, B. V. & Goddard, W. A. Origin of low sodium capacity in graphite and generally weak substrate binding of Na and Mg among alkali and alkaline earth metals. *Proc. Natl Acad. Sci. USA* **113**, 3735–3739 (2016).
- Lv, Y. et al. Interface coupling as a crucial factor for spatial localization of electronic states in a heterojunction of graphene nanoribbons. *Phys. Rev. Appl.* **11**, 024026 (2019).

Acknowledgements

Yuan L. acknowledge the financial support from the Fundamental Research Funds of the Central Universities (Grant No. 531119200076), from Huxiang high level talent program (Grant No. S2018RSCXRC0149), and from the National Natural Science Foundation of China (Grant Nos. 51802090, 61874041, 51991341). Xidong D. acknowledge the support from the National Natural Science Foundation of China (Grant No. 51991343). Z.L. thank Xiao Liu and Gonglei Shao for AFM measurement, and thank Zhiwen Shu for technique support of bending apparatus design.

Author contributions

Yuan L. conceived the research. Yuan L. and Z.L. designed the experiments. Z.L. performed the experiments and data analysis. Yawei L. contributed to DFT simulation. L.R. and L.K. contributed to PL and AFM measurement. Y.Z. and K.C. contributed to FE simulation. Q.T. contributed to the flexible substrate fabrication. J.L., R.W., H.M., B.Z., D.W., and Xidong D. contributed to CVD materials. W.D. and L. L. contributed to the sample fabrication. Xiangfeng D. contributed to manuscript editing. Yuan L. and Z.L. co-

wrote the manuscript. All authors discussed the results and commented on the manuscript.

Competing interests

The authors declare no competing interests.

Additional information

Supplementary information is available for this paper at <https://doi.org/10.1038/s41467-020-15023-3>.

Correspondence and requests for materials should be addressed to Y.L.

Peer review information *Nature Communications* thanks the anonymous reviewer(s) for their contribution to the peer review of this work.

Reprints and permission information is available at <http://www.nature.com/reprints>

Publisher's note Springer Nature remains neutral with regard to jurisdictional claims in published maps and institutional affiliations.



Open Access This article is licensed under a Creative Commons Attribution 4.0 International License, which permits use, sharing, adaptation, distribution and reproduction in any medium or format, as long as you give appropriate credit to the original author(s) and the source, provide a link to the Creative Commons license, and indicate if changes were made. The images or other third party material in this article are included in the article's Creative Commons license, unless indicated otherwise in a credit line to the material. If material is not included in the article's Creative Commons license and your intended use is not permitted by statutory regulation or exceeds the permitted use, you will need to obtain permission directly from the copyright holder. To view a copy of this license, visit <http://creativecommons.org/licenses/by/4.0/>.

© The Author(s) 2020